Nonlinear Dyn
https://doi.org/10.1007/s11071-018-4720-1

ORIGINAL PAPER

Control of linear instabilities by dynamically consistent order reduction on optimally time-dependent modes

Antoine Blanchard · Saviz Mowlavi · Themistoklis P. Sapsis

Received: 25 October 2018 / Accepted: 7 December 2018

Abstract Identification and control of transient instabilities in high-dimensional dynamical systems remain a challenge because transient (non-normal) growth cannot be accurately captured by reduced-order modal analysis. Eigenvalue-based methods classify systems as stable or unstable on the sole basis of the asymptotic behavior of perturbations and therefore fail to predict any short-term characteristics of disturbances, including transient growth. In this paper, we leverage the power of the optimally time-dependent (OTD) modes, a set of time-evolving, orthonormal modes that capture directions in phase space associated with transient and persistent instabilities, to formulate a control law capable of suppressing transient and asymptotic growth around any fixed point of the governing equations. The control law is derived from a reduced-order system resulting from projecting the evolving linearized dynamics onto the OTD modes and enforces that the instantaneous growth of perturbations in the OTD-reduced tangent space be nil. We apply the proposed reduced-order control algorithm to several infinite-dimensional systems, including fluid flows dominated by normal and non-normal instabilities, and demonstrate unequivocal superiority of OTD control over classical modal control.

Keywords Optimally time-dependent modes · Flow control · Non-normal growth · Linear instability

A. Blanchard (✉) · S. Mowlavi (✉) · T. P. Sapsis (✉)
Department of Mechanical Engineering, Massachusetts Institute of Technology, Cambridge, MA 02139, USA
e-mail: ablancha@mit.edu

S. Mowlavi
e-mail: smowlavi@mit.edu

T. P. Sapsis
e-mail: sapsis@mit.edu

1 Introduction

The concept of instability in dynamical systems is generally associated with the spectrum of the linearized operator: a fixed point of the governing equations is stable if and only if all the eigenvalues are confined to the stable part of the complex plane [21]. This approach, referred to as modal stability theory, has led to a number of fundamental results in fluid mechanics pertaining to parallel shear flows [27,28], compressible boundary layers [25], elliptical instabilities [6,31], bluff body flows [34,47], and many more. But it took the scientific community several decades to realize that the modal perspective provides information on stability of a base flow only in the asymptotic limit and therefore fails to capture features associated with transient (non-normal) growth of perturbations. Episodes of transient growth are attributable to the non-normality of the linearized operator and may occur even when the latter has no unstable eigenvalues. For example, in many wall-bounded shear flows, eigenvalue analysis predicts a critical value of the Reynolds number for transition well above that observed experimentally [41]. The recognition that short-term instabilities play a critical role

Published online: 17 December 2018

in fluid dynamical systems [38], but also in climate dynamics [14,29] and thermoacoustics [5], has then led to a large number of studies focused on finding disturbances that maximize energy amplification over a finite-time horizon [17,35]. These "optimal" disturbances, which grow the most over a short timescale, differ significantly from the least stable eigenvectors of the system, so much so that even in simple situations involving transition to turbulence, non-modal stability analysis paints a much more complete picture than conventional modal analysis.

By now, the theory of non-normal instability has matured to the point where it can be incorporated into control algorithms. Flow control is a rapidly expanding field, and one of the challenges it faces is that of dimensionality. Controlling high-dimensional systems such as fluid flows is often prohibitively expensive as many control strategies do not scale well with the dimension of the system [2]. With machine learning control still in an embryonic stage [12], order reduction techniques have become customary, because they allow construction of low-dimensional subspaces in which design and implementation of controllers are computationally tractable [44]. Some methods have been around for decades, such as proper orthogonal decomposition (POD) [24], and others have been developed more recently, such as balanced truncation [26], balanced proper orthogonal decomposition (BPOD) [36], the eigensystem realization algorithm (ERA) [23], and dynamic mode decomposition (DMD) [33,39], often with a view to making the method data-driven. But even the most sophisticated reduced-order models struggle with capturing non-normal instabilities. POD performs extremely poorly for systems exhibiting large transient growth [11], while DMD, BPOD, and ERA, or combinations thereof, often require subspaces with double-digit dimension to achieve acceptable errors, even in configurations as simple as plane Poiseuille flow [37].

In this work, we elect the optimally time-dependent (OTD) modes, recently introduced by Babaee and Sapsis [4], to reduce the system dimensionality in a dynamically consistent fashion, that is, one that preserves features of the full-order system associated with transient and persistent instabilities. The OTD modes are a set of orthonormal vectors that *adaptively* track directions in phase space responsible for transient growth and instabilities [3,4]. The results of Babaee and Sapsis [4] showed that a very small number of OTD modes are capable of capturing transient *and* asymptotic instabilities, which led the authors to surmise that the OTD framework is particularly appropriate to design reduced-order control algorithms toward suppression of transient instabilities. The purpose of the present work is precisely to develop a control strategy centered around the OTD modes. To this end, we design a feedback control law that suppresses instantaneous growth of perturbations in the OTD-reduced tangent space of the linearized dynamics. The end result is a control algorithm that fulfills all of the aforementioned requirements related to low dimensionality and non-normality.

The paper is structured as follows. We present the problem and review the concept of OTD modes in Sect. 2, formulate an OTD-based control law in Sect. 3, apply the proposed control strategy to several dynamical systems in Sect. 4, and offer some conclusions in Sect. 5.

2 Preliminaries

2.1 Formulation of the problem

We consider a generic dynamical system whose evolution obeys

$$\dot{z} = \mathscr{F}(z), \tag{2.1}$$

where z belongs to an appropriate function space $\mathcal{X}$, $\mathscr{F}$ is a nonlinear differential operator, and overdot denotes partial differentiation with respect to the time variable t. We specify the initial condition at time t_0 as $z(\cdot, t_0) = z_0$. We assume that (2.1) admits at least one fixed point, that is, the set $\{z \in \mathcal{X} : \mathscr{F}(z) = 0\}$ is not empty. We denote by z_e any fixed point of (2.1), regardless of how many there are. Infinitesimal perturbations about a trajectory obey the variational equations

$$\dot{v} = \mathscr{L}(z; v), \tag{2.2}$$

where $v \in \mathcal{X}$, and $\mathscr{L}(z; v) = \mathrm{d}\mathscr{F}(z; v)$ is the Gâteaux derivative of $\mathscr{F}$ evaluated at z along the direction v. We will find it useful, and sometimes more intuitive, to consider (2.1) and (2.2) in a finite-dimensional setting, that is,

$$\dot{\mathbf{z}} = \mathbf{F}(\mathbf{z}), \quad \mathbf{z} \in \mathbb{R}^d \tag{2.3a}$$

and

$$\dot{\mathbf{v}} = \mathbf{L}(\mathbf{z})\mathbf{v}, \quad \mathbf{v} \in \mathbb{R}^d, \tag{2.3b}$$

where $\mathbf{F} : \mathbb{R}^d \to \mathbb{R}^d$ is a smooth vector field and $\mathbf{L}(\mathbf{z}) = \nabla_{\mathbf{z}}\mathbf{F}(\mathbf{z}) \in \mathbb{R}^{d\times d}$ is the Jacobian matrix associated with $\mathbf{F}$ evaluated at $\mathbf{z}$. The finite-dimensional formulation may be viewed as the result of projecting the infinite-dimensional system onto a finite-dimensional set of complete functions and for our purposes does not restrict the scope of the analysis.

Here, we consider situations in which infinitesimal perturbations from a fixed point of the governing equations experience significant transient (and possibly asymptotic) growth, which we wish to suppress by a suitably designed control algorithm. The challenge is to formulate a control strategy that is low dimensional and capable of suppressing instabilities resulting from normal *and* non-normal behavior. The first requirement may be satisfied by projecting the dynamics onto a carefully selected subspace with dimension much smaller than that of the phase space and applying the control algorithm in the reduced-order subspace. One candidate subspace is the unstable eigenspace $\mathcal{E}_u$ of $\mathscr{L}_e = \mathscr{L}(z_e;\cdot)$, whose eigenvalues dictate linear stability of z_e. However, the subspace $\mathcal{E}_u$ provides an indication regarding exponential growth of perturbations about z_e only in the asymptotic limit $t \to +\infty$ and therefore fails to capture any short-term features of the trajectory. In particular, eigenvalues of $\mathscr{L}_e$ may predict linear stability for z_e, even when significant transient growth occurs. A well-known example of such behavior is found in fluid mechanics with plane Poiseuille flow (parallel flow between two plates; see Sect. 4.2.2). For this flow, a "naive" eigenvalue calculation around the base state predicts a critical value of the Reynolds number (based on the centerline velocity of the undisturbed flow and the channel half-width) for transition well above that observed experimentally. This is because the eigenvalue approach is unable to capture the non-normal nature of the linearized operator, which is responsible for the significant transient growth seen in experiments and computations. This result is significant, because non-normal growth can activate nonlinear mechanisms triggering turbulence, and a mere inspection of the spectrum of $\mathscr{L}_e$ cannot explain that outcome.

Therefore, it is clear that suppression of transient growth and instabilities cannot be achieved by a control algorithm solely based on eigenvalue considerations of $\mathscr{L}_e$. Data-driven approaches, such as proper orthogonal decomposition [22,24,43] and dynamic mode decomposition [39], may look like attractive alternatives, but the modes produced by such decompositions are time independent and intrinsically "biased" toward the data that were used to generate them, so they cannot *adapt* to directions associated with transient instabilities as the trajectory wanders about in the phase space and experiences various dynamical regimes. On the other hand, the optimally time-dependent (OTD) modes, recently introduced by Babaee and Sapsis [4], provide a promising framework for our control problem. We review the reasons why below.

2.2 Review of the optimally time-dependent (OTD) modes

The concept of OTD modes was first introduced in Babaee and Sapsis [4] in the form of a constrained minimization problem,

$$\min_{\dot{u}_i} \sum_{i=1}^{r} \|\dot{u}_i - \mathscr{L}(z;u_i)\|^2 \ \text{ subject to } \langle u_i, u_j\rangle = \delta_{ij}, \tag{2.4}$$

where $\langle\cdot,\cdot\rangle$ is a suitable inner product and $\|\cdot\|$ the induced norm, δ_{ij} is the Kronecker delta, and $u_i \in \mathcal{X}$ is the ith OTD mode. The r-dimensional subspace spanned by the collection $\{u_i\}_{i=1}^r$ is referred to as the OTD subspace. Because of the orthonormality constraint in (2.4), the set $\{u_i\}_{i=1}^r$ trivially forms an orthonormal basis of the OTD subspace. We note that the optimization in (2.4) is performed with respect to $\dot{u}_i$ and not u_i, so the OTD modes are by construction the best approximation of the linearized dynamics in the subspace that they span.

As discussed in Babaee and Sapsis [4], the minimization problem (2.4) is equivalent to a set of coupled partial differential equations governing the evolution of each OTD mode. For the dynamical system (2.1) and an r-dimensional OTD subspace, the ith OTD mode obeys

$$\dot{u}_i = \mathscr{L}(z;u_i) - \sum_{k=1}^{r} [\langle \mathscr{L}(z;u_i), u_k\rangle u_k - \Phi_{ik}u_k], \quad 1 \le i \le r, \tag{2.5}$$

where $\mathbf{\Phi} = (\Phi_{ik})_{i,k=1}^r \in \mathbb{R}^{r\times r}$ is any skew-symmetric tensor (i.e., such that $\Phi_{ik} = -\Phi_{ki}$ for all $1 \le i, k \le r$). The choice of $\mathbf{\Phi}$ does not affect the OTD subspace, since any two initially equivalent subspaces propagated

with (2.5), each with a different choice of $\mathbf{\Phi}$, remain equivalent for all times [4]. A natural candidate for $\mathbf{\Phi}$ is the zero tensor, but that leads to a fully coupled system of OTD equations in which all r modes appear in each equation of (2.5). In contrast, choosing $\mathbf{\Phi}$ such that

$$\Phi_{ik} = \begin{cases} -\langle \mathscr{L}(z; u_k), u_i \rangle, & k < i \\ 0, & k = i \\ \langle \mathscr{L}(z; u_i), u_k \rangle, & k > i \end{cases} \tag{2.6}$$

leads to a system in which the equation for the ith mode depends only on the previous modes u_j with index $1 \leq j \leq i$. With this choice of $\mathbf{\Phi}$, the equation for the ith OTD mode reads

$$\begin{aligned} \dot{u}_i = {} & \mathscr{L}(z; u_i) - \langle \mathscr{L}(z; u_i), u_i \rangle u_i \\ & - \sum_{k=1}^{i-1} [\langle \mathscr{L}(z; u_i), u_k \rangle \\ & + \langle \mathscr{L}(z; u_k), u_i \rangle] u_k, \quad 1 \leq i \leq r, \end{aligned} \tag{2.7}$$

and the system assumes a lower triangular form, readily solvable by forward substitution. [We note that the summation index goes to $i-1$ in (2.7), rather than r as in (2.5)]. In finite dimension, we introduce the matrix $\mathbf{U} \in \mathbb{R}^{d \times r}$ whose ith column is $\mathbf{u}_i$ and write the finite-dimensional counterpart of (2.5) in compact form as

$$\dot{\mathbf{U}} = \mathbf{L}(\mathbf{z})\mathbf{U} - \mathbf{U}\left[\mathbf{U}^{\intercal}\mathbf{L}(\mathbf{z})\mathbf{U} - \mathbf{\Phi}\right], \tag{2.8}$$

where $\intercal$ denotes the Hermitian transpose operator.

Of the numerous properties that have been established for the OTD modes, we review a few relevant to the present work. First, the OTD modes span the same flow-invariant subspace as the solutions $\{v_i(t)\}_{i=1}^{r}$ of the variational equations (2.2), while preserving orthonormality for all times [16]. Second, for a hyperbolic fixed point z_e, the OTD subspace is asymptotically equivalent to the most unstable eigenspace of the linearized operator $\mathscr{L}_e$ [4]. Third, for a time-dependent trajectory, the OTD subspace aligns exponentially rapidly with the eigendirections of the left Cauchy–Green tensor associated with transient instabilities [3].

The above properties imply that an r-dimensional OTD subspace continually seeks out the r-dimensional subspace that is most rapidly growing in the tangent space (i.e., the space where perturbations "live"). Therefore, because of the orthonormality constraint, the OTD modes provide a numerically stable and inexpensive tool for computing finite- and infinite-time Lyapunov exponents along a given trajectory. We also note that the OTD modes coincide with the backward Lyapunov vectors (also known as Gram–Schmidt vectors) and hence converge at long times to a well-defined basis that depends only on the state of the system in the phase space, and not on the history of the trajectory prior to reaching the attractor [8]. But perhaps the most appealing property of the OTD modes is their unique ability to capture transient episodes of intense growth, regardless of the exponential or non-normal origin of the latter [4]. Because of their time-dependent nature, the OTD modes are able to "track" the most unstable directions in the phase space along a given trajectory and therefore are a natural candidate for the formulation of a reduced-order control algorithm.

3 Formulation of an OTD-based control law

In this section, we formulate a control law based on the OTD framework in order to suppress episodes of transient growth around a fixed point of the governing equations. The analytical exposition is done in finite dimension, but carries over to the infinite-dimensional case.

3.1 Formulation of the control problem

We consider the system (2.3a) subject to a control force,

$$\dot{\mathbf{z}} = \mathbf{F}(\mathbf{z}) + \mathbf{B}\mathbf{c}, \tag{3.1}$$

where $\mathbf{c} \in \mathbb{R}^p$ is the control variable and $\mathbf{B} \in \mathbb{R}^{d \times p}$ is the control action matrix. The control force $\mathbf{f}_c = \mathbf{B}\mathbf{c}$ may be seen as a body force acting on the system. Since we are interested in steering the trajectory $\mathbf{z}$ toward a fixed point $\mathbf{z}_e$, we introduce the quantity $\mathbf{z}' = \mathbf{z} - \mathbf{z}_e$ describing the deviation of the current state from the target state. The controlled perturbation $\mathbf{z}'$ then obeys

$$\dot{\mathbf{z}}' = \mathbf{L}(\mathbf{z})\mathbf{z}' + \mathbf{B}\mathbf{c} + O\left(\|\mathbf{z}'\|^2\right), \tag{3.2}$$

where we have used the fact that $\mathbf{L}(\mathbf{z_e}) = \mathbf{L}(\mathbf{z}) + O(\|\mathbf{z}'\|)$. Assuming that the higher-order terms in (3.2) are sufficiently small that they may be neglected, we arrive at the controlled variational equation

$$\dot{\mathbf{z}}' = \mathbf{L}(\mathbf{z})\mathbf{z}' + \mathbf{B}\mathbf{c}, \tag{3.3}$$

which will be the basis for our analysis. In the majority of industrial applications, the dimension of equation (3.3) is very large (typically, millions of degrees of

freedom), and designing a controller for a wide range of parameters often is a computationally onerous task. A promising approach is to proceed to an order reduction of the dynamics, which is generally done by a Galerkin projection of the governing equations onto an appropriate basis; for example, POD modes computed from a collection of snapshots of the trajectory, or eigenfunctions of the linear operator $\mathbf{L}_e = \mathbf{L}(\mathbf{z}_e)$. In the following, we give arguments in favor of projecting the dynamics onto OTD modes, rather than any other candidate basis.

3.2 Order reduction of the dynamics by OTD modes

As discussed in Sect. 2.2, the OTD modes span flow-invariant subspaces of the tangent space, so they can be used to reduce the dimensionality of the linear operator $\mathbf{L}$ in a *dynamically consistent fashion* [16]. To see this, we consider a solution $\mathbf{v} \in \mathbb{R}^d$ of the original variational equation (2.3b), and its projection $\boldsymbol{\eta} \in \mathbb{R}^r$ onto the OTD basis $\mathbf{U}$,

$$\boldsymbol{\eta}(t) = \mathbf{U}(t)^\intercal \mathbf{v}(t), \quad \mathbf{v} \in \mathrm{span}(\mathbf{U}). \tag{3.4}$$

Here, the OTD basis $\mathbf{U}$ evolves according to the OTD equation (2.8) along the trajectory $\mathbf{z}(t)$ of the system. (The dependence on time is shown explicitly to emphasize this point). The vector $\boldsymbol{\eta}$ represents the solution $\mathbf{v}$ expressed in the OTD basis. We also have that $\mathbf{v} = \mathbf{U}\boldsymbol{\eta}$ as a result of the orthonormality of the OTD modes. Substituting in (2.3b) yields the reduced linear equation

$$\dot{\boldsymbol{\eta}} = \left(\mathbf{U}^\intercal \mathbf{L}\mathbf{U} - \boldsymbol{\Phi}\right)\boldsymbol{\eta}. \tag{3.5}$$

Conversely, if $\boldsymbol{\eta}$ solves the reduced equation (3.5), then $\mathbf{v} = \mathbf{U}\boldsymbol{\eta}$ solves the original equation (2.3b), which is the other prerequisite for dynamically consistent reduction. We note that the condition $\mathbf{v} \in \mathrm{span}(\mathbf{U})$ implies that any direction orthogonal to $\mathbf{U}$ is left out by the order reduction. This point is discussed in greater detail in Sect. 3.4. The linear map $\mathbf{L}_r : \mathbb{R}^r \to \mathbb{R}^r$ defined as

$$\mathbf{L}_r = \mathbf{U}^\intercal \mathbf{L}\mathbf{U} - \boldsymbol{\Phi} \tag{3.6}$$

is referred to as the *reduced linear operator*. As discussed in Farazmand and Sapsis [16], the OTD order reduction carries over to the infinite-dimensional case, since projection of the infinite-dimensional operator $\mathscr{L}$ to an r-dimensional OTD subspace $\{u_i\}_{i=1}^r$ yields a reduced linear operator that is *finite-dimensional* (i.e., an $r \times r$ matrix), whose entries are given by

$$[\mathbf{L}_r]_{ij} = \langle u_i, \mathscr{L}(z; u_j)\rangle - \Phi_{ij}, \quad 1 \le i, j \le r. \tag{3.7}$$

A great advantage of the OTD order reduction is that it retains the information of the full-order solution associated with transient instabilities, irrespective of the modal or non-modal character of the latter. This is because the OTD modes capture the most unstable directions in phase space, and since they are computed along an evolving trajectory, they are able to adapt to the various regions visited by the system. Therefore, the OTD modes establish themselves as a natural and relevant candidate for the projection basis.

We now return to the control problem (3.3) and apply the order reduction ideas described above. We define a reduced control matrix $\mathbf{B}_r \in \mathbb{R}^{r\times p}$ as

$$\mathbf{B}_r = \mathbf{U}^\intercal \mathbf{B}, \tag{3.8}$$

and obtain the reduced controlled variational equation,

$$\dot{\boldsymbol{\eta}} = \mathbf{L}_r(\mathbf{z})\boldsymbol{\eta} + \mathbf{B}_r \mathbf{c}, \tag{3.9}$$

where we have let $\boldsymbol{\eta} = \mathbf{U}^\intercal \mathbf{z}'$. Equation (3.9) is a set of r ordinary differential equations, making it much cheaper to compute an appropriate reduced action matrix $\mathbf{B}_r$. We emphasize that we have thus far made no assumption regarding the form of the reduced control force $\mathbf{f}_{r,c} = \mathbf{U}^\intercal \mathbf{f}_c$. To guarantee dynamic consistency of the order reduction, we only require that $\mathbf{f}_c \in \mathrm{span}(\mathbf{U})$, that is, $\mathbf{f}_c = \mathbf{U}\mathbf{f}_{r,c}$, but the choice of $\mathbf{f}_{r,c}$ remains arbitrary. So here, the OTD modes have been used merely to reduce the dimensionality of the system in a consistent fashion (i.e., by preserving instability properties of the full-order system), and this gives us complete freedom in the choice of the control scheme inside the OTD subspace (e.g., linear quadratic regulator or proportional–integral-derivative controller). We now explore how the OTD modes may be incorporated in a control scheme to suppress transient instabilities in the reduced-order system.

3.3 Formulation of a control law

Inspired by the theory of proportional control, in which the controller output is proportional to the error, we seek a closed-loop feedback control law in the form $\mathbf{c} = \mathbf{K}_r\boldsymbol{\eta}$, where $\mathbf{K}_r \in \mathbb{R}^{p\times r}$ is the reduced feedback gain matrix. We recall that $\boldsymbol{\eta} = \mathbf{U}^\intercal \mathbf{z}' = \mathbf{U}^\intercal(\mathbf{z} - \mathbf{z}_e)$ is nothing more than the deviation of the trajectory $\mathbf{z}$ from the fixed point $\mathbf{z}_e$ expressed in the OTD basis $\mathbf{U}$, so our goal is to find an appropriate $\mathbf{K}_r$ that drives the reduced

perturbation $\boldsymbol{\eta}$ to $\mathbf{0}$. With this in hand, the controlled reduced system (3.9) becomes

$$\dot{\boldsymbol{\eta}} = \mathbf{L}_{r,c}\boldsymbol{\eta}, \tag{3.10}$$

where $\mathbf{L}_{r,c} = \mathbf{L}_r + \mathbf{B}_r\mathbf{K}_r$ is the *closed-loop reduced linear operator*. (We will sometimes refer to $\mathbf{L}_r$ as the *open-loop* reduced linear operator). The operator $\mathbf{L}_{r,c}$ (and $\mathbf{L}_r$ for that matter) depends on time, so its eigenvalues may not be used to determine growth or decay of the solution $\boldsymbol{\eta}$. Instead, we consider the instantaneous growth of the perturbation in the OTD subspace,

$$\frac{1}{2}\frac{\mathrm{d}}{\mathrm{d}t}\|\boldsymbol{\eta}\|^2 = \frac{\langle \mathbf{L}_{r,c}\boldsymbol{\eta}, \boldsymbol{\eta}\rangle + \langle \boldsymbol{\eta}, \mathbf{L}_{r,c}\boldsymbol{\eta}\rangle}{2} = \langle \boldsymbol{\eta}, \mathbf{S}_{r,c}\boldsymbol{\eta}\rangle, \tag{3.11}$$

where $\mathbf{S}_{r,c}$ is the symmetric part of $\mathbf{L}_{r,c}$. We note that $\mathbf{S}_{r,c}$ may be expressed in terms of the symmetric part $\mathbf{S}_r$ of $\mathbf{L}_r$, because

$$\begin{aligned}\mathbf{S}_{r,c} &= \frac{\mathbf{L}_{r,c} + \mathbf{L}_{r,c}^\intercal}{2} = \frac{\mathbf{L}_r + \mathbf{L}_r^\intercal}{2} + \frac{\mathbf{B}_r\mathbf{K}_r + \mathbf{K}_r^\intercal\mathbf{B}_r^\intercal}{2} \\ &= \mathbf{S}_r + \frac{\mathbf{B}_r\mathbf{K}_r + \mathbf{K}_r^\intercal\mathbf{B}_r^\intercal}{2}.\end{aligned} \tag{3.12}$$

For the norm of the perturbation to become vanishingly small, we require the yet undetermined feedback matrix $\mathbf{K}_r$ to be such that

$$\forall \boldsymbol{\eta} \neq \mathbf{0}, \quad \frac{1}{2}\frac{\mathrm{d}}{\mathrm{d}t}\|\boldsymbol{\eta}\|^2 < 0, \tag{3.13}$$

so $\mathbf{S}_{r,c}$ must be negative definite by virtue of (3.11). Since negative definiteness is a condition on the spectrum of the operator, it is convenient to introduce the eigendecomposition $\mathbf{S}_r = \mathbf{R}\boldsymbol{\Lambda}_r\mathbf{R}^\intercal$, where $\mathbf{R} \in \mathbb{R}^{r\times r}$ is a unitary rotation matrix containing the eigenvectors of $\mathbf{S}_r$, and $\boldsymbol{\Lambda}_r = \mathrm{diag}(\lambda_i) \in \mathbb{R}^{r\times r}$ is a diagonal matrix containing the real eigenvalues of $\mathbf{S}_r$, ordered from most (λ_1) to least (λ_r) unstable. We may use the eigenbasis of $\mathbf{S}_r$ to define a rotated closed-loop symmetric operator as

$$\hat{\mathbf{S}}_{r,c} = \boldsymbol{\Lambda}_r + \frac{\mathbf{R}^\intercal\mathbf{B}_r\mathbf{K}_r\mathbf{R} + \mathbf{R}^\intercal\mathbf{K}_r^\intercal\mathbf{B}_r^\intercal\mathbf{R}}{2}, \tag{3.14}$$

where it is understood that $\hat{\mathbf{S}}_{r,c} = \mathbf{R}^\intercal\mathbf{S}_{r,c}\mathbf{R}$. The control problem may now be formulated as finding a feedback matrix $\mathbf{K}_r$ such that $\hat{\mathbf{S}}_{r,c}$ is negative definite.

Control problem *Given a time-dependent diagonal reduced matrix $\boldsymbol{\Lambda}_r \in \mathbb{R}^{r\times r}$, a reduced control matrix $\mathbf{B}_r \in \mathbb{R}^{r\times p}$, and a unitary rotation matrix $\mathbf{R} \in \mathbb{R}^{r\times r}$, find a reduced feedback matrix $\mathbf{K}_r \in \mathbb{R}^{p\times r}$ such that the rotated closed-loop symmetric operator $\hat{\mathbf{S}}_{r,c}$ is negative definite.*

To minimize the cost of the control scheme, we additionally require that the norm of the matrix $\mathbf{K}_r$ be minimized. We also note that at this point still, we have used the OTD modes for nothing other than the order reduction of the linearized dynamics.

The next step in the analysis is to solve the above control problem and find an expression for the matrix $\mathbf{K}_r$. We now make two critical assumptions. First, we assume that the control matrix $\mathbf{B}$ is equal to the identity matrix, so the control vector $\mathbf{c}$ has as many inputs as there are state variables (i.e., $p = d$). In words, this means that the control can act everywhere on the state of the system. With this assumption, we immediately see that $\mathbf{B}_r = \mathbf{U}^\intercal$, and the matrix $\hat{\mathbf{S}}_{r,c}$ becomes

$$\hat{\mathbf{S}}_{r,c} = \boldsymbol{\Lambda}_r + \frac{\mathbf{R}^\intercal\mathbf{U}^\intercal\mathbf{K}_r\mathbf{R} + \mathbf{R}^\intercal\mathbf{K}_r^\intercal\mathbf{U}\mathbf{R}}{2}, \tag{3.15}$$

with $\mathbf{K}_r$ now in $\mathbb{R}^{d\times r}$. Second, as discussed in Sect. 3.2, we require that the control vector $\mathbf{c}$ belongs to the OTD subspace, meaning that there exists a matrix $\mathbf{A}_r \in \mathbb{R}^{r\times r}$ such that $\mathbf{K}_r = \mathbf{U}\mathbf{A}_r$. The matrix $\mathbf{A}_r \in \mathbb{R}^{r\times r}$ may be chosen arbitrarily. Any symmetric matrix is a good choice for $\mathbf{A}_r$, because it considerably simplifies the expression for $\hat{\mathbf{S}}_{r,c}$,

$$\hat{\mathbf{S}}_{r,c} = \boldsymbol{\Lambda}_r + \mathbf{R}^\intercal\mathbf{A}_r\mathbf{R}, \quad \mathbf{A}_r = \mathbf{A}_r^\intercal. \tag{3.16}$$

Now that $\hat{\mathbf{S}}_{r,c}$ has been expressed as the sum of a diagonal open-loop component $\boldsymbol{\Lambda}_r$ and a symmetric rotated feedback component $\mathbf{R}^\intercal\mathbf{A}_r\mathbf{R}$, the control problem is straightforward to solve. Indeed, since $\boldsymbol{\Lambda}_r$ is diagonal, it is easy to design $\mathbf{R}^\intercal\mathbf{A}_r\mathbf{R}$ and, hence, $\mathbf{K}_r$ so that $\hat{\mathbf{S}}_{r,c}$ is negative definite while minimizing the cost $\|\mathbf{K}_r\|$. (It should be clear that $\|\mathbf{K}_r\| = \|\mathbf{A}_r\| = \|\mathbf{R}^\intercal\mathbf{A}_r\mathbf{R}\|$). The optimal solution is given by

$$\mathbf{A}_r = \mathbf{R}\mathrm{diag}[-(\lambda_i + \zeta)\mathscr{H}(\lambda_i)]\mathbf{R}^\intercal, \tag{3.17}$$

where $\mathscr{H}$ is the Heaviside function and $\zeta \in \mathbb{R}^+$ is a damping parameter. The Heaviside function guarantees that the control acts only on directions associated with positive instantaneous growth (those with $\lambda_i \geq 0$), and the parameter ζ governs the intensity with which each of these directions is damped. With $\mathbf{A}_r$ chosen according to (3.17), the rate of change in the perturbation magnitude in closed loop is simply

$$\frac{1}{2}\frac{\mathrm{d}}{\mathrm{d}t}\|\boldsymbol{\eta}\|^2 = \left\langle \boldsymbol{\eta}, \mathbf{R}\hat{\mathbf{S}}_{r,c}\mathbf{R}^{\mathsf{T}}\boldsymbol{\eta}\right\rangle = -\zeta\sum_{\lambda_i\geq 0}\hat{\eta}_i^2 + \sum_{\lambda_i<0}\lambda_i\hat{\eta}_i^2, \tag{3.18}$$

where we have defined the rotated perturbation $\hat{\boldsymbol{\eta}} = \mathbf{R}^{\mathsf{T}}\boldsymbol{\eta} = \hat{\eta}_i\mathbf{e}_i$. It should be clear from (3.18) that $\mathrm{d}\|\boldsymbol{\eta}\|^2/\mathrm{d}t < 0$ for all $\boldsymbol{\eta} \neq \mathbf{0}$, ensuring that $\mathbf{z}$ tends to $\mathbf{z}_e$ at long times.

Collecting the pieces, we arrive at the final expression for the control force,

$$\mathbf{f}_c = \mathbf{U}\mathbf{R}\mathrm{diag}[-(\lambda_i+\zeta)\mathscr{H}(\lambda_i)]\mathbf{R}^{\mathsf{T}}\mathbf{U}^{\mathsf{T}}(\mathbf{z}-\mathbf{z}_e), \tag{3.19}$$

which may be substituted in place of $\mathbf{Bc}$ in the original full-order nonlinear system (3.1). The control force $\mathbf{f}_c$ is defined for all $\mathbf{z}\in\mathbb{R}^d$ and all times $t \geq t_0$, that is, it acts as a body force on every state variable of the system. We address the issue of restricting the range of the OTD controller in [9].

3.4 Properties of the OTD control scheme

We now discuss several issues related to the proposed OTD control scheme. Three key questions arise. First, how should the OTD subspace be initialized? Second, how should the dimension of the OTD subspace be chosen? Third, what is the scope of validity of the proposed control algorithm?

3.4.1 Initialization of the OTD subspace

For the OTD reduction $\mathbf{z}' = \mathbf{U}\boldsymbol{\eta}$ to be consistent, it is critical that the initial deviation $\mathbf{z}'(t_0) = \mathbf{z}(t_0) - \mathbf{z}_e$ have a nonzero projection on the OTD subspace, that is, $\mathbf{U}(t_0)^{\mathsf{T}}\mathbf{z}'(t_0) \neq \mathbf{0}$. This can be realized in a number of ways. One option is to let $\mathbf{U}(t_0) = \{\tilde{\mathbf{z}}'(t_0), \tilde{\mathbf{w}}_1, \ldots, \tilde{\mathbf{w}}_{r-1}\}$, where $\tilde{\mathbf{z}}'(t_0) = \mathbf{z}'(t_0)/\|\mathbf{z}'(t_0)\|$ is the normalized initial perturbation, and $\tilde{\mathbf{w}}_i$ is the ith leading eigenvector of $(\mathbf{L}_e + \mathbf{L}_e^{\mathsf{T}})/2$ orthonormalized against the set $\{\tilde{\mathbf{z}}'(t_0), \tilde{\mathbf{w}}_1, \ldots, \tilde{\mathbf{w}}_{i-1}\}$. In this way, the OTD subspace initially contains the initial perturbation, as well as the directions associated with largest instantaneous growth for the steady operator $\mathbf{L}_e$.

Another option is given by Babaee and Sapsis [4], who suggested to use the r leading right singular vectors of the propagator $\mathbf{M}(t_0, t_{\max})$. Those vectors are essentially a set of r optimal initial conditions that reach maximum possible amplification at a given time $t_{\max}$. This is a good choice because the right singular vectors of $\mathbf{M}(t_0, t_{\max})$ are real and orthonormal, and they are associated with maximum amplification over the finite-time horizon $[t_0, t_{\max}]$.

We note that in the above two approaches, the OTD modes satisfy the boundary conditions at $t = t_0$, as well as any constraint appearing in the linearized equations such as incompressibility. In practice, however, this need not be the case, and the OTD subspace may be initialized arbitrarily. For example, we may choose a Fourier basis, or a set of Legendre polynomials, which we are careful to orthonormalize. The key point with such initialization is to make sure that the OTD subspace contains the directions of instantaneous growth of the initial perturbation, which is generally true except in pathological cases.

3.4.2 Dimension of the OTD subspace

To determine what the dimension r of the OTD subspace should be for the control to be efficient, we first note that r governs how faithful the order reduction of the linear operator $\mathbf{L}$ is to the full-order dynamics, or in other words, how much information is lost upon projection onto the OTD subspace. So r must be chosen on the basis of the information we wish to retain in the reduced-order equation. In the present context of controlling instabilities, we must select r so that the reduced system (3.5) encapsulates all the information related to transient and asymptotic growth. Should r be too small, the OTD reduction would leave out directions associated with instabilities, which the control law would in turn be unable to suppress.

For normal (i.e., modal) operators, it is sufficient to capture directions associated with exponential growth, that is, the unstable eigendirections of the operator $\mathbf{L}_e$. This means that we must choose $r \geq \dim\mathcal{E}_u$. In doing so, we guarantee that the unstable eigenspaces of $\mathbf{L}_e$ and $\mathbf{U}^{\mathsf{T}}\mathbf{L}_e\mathbf{U}$ coincide, by virtue of the following theorem.

Theorem 1 *Let $\mathbf{Q}\in\mathbb{R}^{d\times d}$, and let $\boldsymbol{\Pi}\in\mathbb{R}^{r\times d}$ be a projector such that $\boldsymbol{\Pi}\boldsymbol{\Pi}^{\mathsf{T}} = \mathbf{I}_r$. Then, the following holds.*

1. *If $(\mu, \boldsymbol{\psi})$ is an eigenpair of $\boldsymbol{\Pi}\mathbf{Q}\boldsymbol{\Pi}^{\mathsf{T}}$, and $\mathrm{range}(\boldsymbol{\Pi}^{\mathsf{T}})$ is an eigenspace of $\mathbf{Q}$, then $(\mu, \boldsymbol{\Pi}^{\mathsf{T}}\boldsymbol{\psi})$ is an eigenpair of $\mathbf{Q}$.*
2. *If $(\mu, \boldsymbol{\theta})$ is an eigenpair of $\mathbf{Q}$, and $\boldsymbol{\theta}$ is in $\mathrm{range}(\boldsymbol{\Pi}^{\mathsf{T}})$, then $(\mu, \boldsymbol{\Pi}\boldsymbol{\theta})$ is an eigenpair of $\boldsymbol{\Pi}\mathbf{Q}\boldsymbol{\Pi}^{\mathsf{T}}$.*

Proof The proof of the above two items is as follows.

1. Since range($\mathbf{\Pi}^\intercal$) is an eigenspace of $\mathbf{Q}$, we have that for any $\mathbf{a} \in \mathbb{R}^r$, there exists $\mathbf{b} \in \mathbb{R}^r$ such that $\mathbf{Q\Pi}^\intercal\mathbf{a} = \mathbf{\Pi}^\intercal\mathbf{b}$. This means that $\mathbf{\Pi Q\Pi}^\intercal\mathbf{a} = \mathbf{b}$. Suppose now that $\mathbf{a} = \boldsymbol{\psi}$ is an eigenvector of $\mathbf{\Pi Q\Pi}^\intercal$, and let μ be the associated eigenvalue. Then, by definition, $\mathbf{\Pi Q\Pi}^\intercal\boldsymbol{\psi} = \mu\boldsymbol{\psi}$, and so $\mathbf{b} = \mu\boldsymbol{\psi}$. We thus obtain $\mathbf{Q\Pi}^\intercal\boldsymbol{\psi} = \mu\mathbf{\Pi}^\intercal\boldsymbol{\psi}$, which completes the proof of item 1.
2. Since $\boldsymbol{\theta} \in$ range($\mathbf{\Pi}^\intercal$), there exists $\mathbf{b} \in \mathbb{R}^r$ such that $\boldsymbol{\theta} = \mathbf{\Pi}^\intercal\mathbf{b}$. Also, since by definition $\mathbf{Q}\boldsymbol{\theta} = \mu\boldsymbol{\theta}$, we have $\mathbf{Q\Pi}^\intercal\mathbf{b} = \mu\mathbf{\Pi}^\intercal\mathbf{b}$. Pre-multiplying by $\mathbf{\Pi}$, we obtain $\mathbf{\Pi Q\Pi}^\intercal\mathbf{b} = \mu\mathbf{b}$. Equivalently, we may write $\mathbf{\Pi Q\Pi}^\intercal\mathbf{\Pi}\boldsymbol{\theta} = \mu\mathbf{\Pi}\boldsymbol{\theta}$, which completes the proof of item 2. □

We note that for $\mathbf{\Pi}^\intercal = \mathbf{U}$, the assumptions related to range($\mathbf{\Pi}^\intercal$) are trivially satisfied asymptotically when the linearized operator is steady. We also note that Theorem 1 provides an illustration of the fact that the OTD reduction is dynamically consistent, that is, projection of a steady operator on the OTD modes does not alter the spectral content of the operator in the asymptotic limit.

For non-normal (i.e., non-modal) operators, it is not sufficient to consider $\dim \mathcal{E}_u$ because non-normal growth does not necessarily take place along the unstable eigendirections. For a simple example, we consider the matrix

$$\mathbf{L}_e = \begin{bmatrix} -1 & 5 \\ 0 & -2 \end{bmatrix}, \tag{3.20}$$

whose eigenvalues indicate asymptotic stability, whereas those of its symmetric part reveal significant non-normal growth along the direction $((1 - \sqrt{26})/5, 1)^\intercal$. So to capture (and later suppress) transient growth, the dimension of the OTD subspace must be such that $r \geq \dim \mathcal{E}_u^s$, where $\mathcal{E}_u^s$ is the unstable eigenspace of $(\mathbf{L}_e + \mathbf{L}_e^\intercal)/2$.

If we now consider the matrix (3.20) in which the signs of the diagonal elements have been changed, the eigenvalues of the resulting operator are positive (1 and 2), but the eigenvalues of its symmetric part have opposite signs (about -2.01 and 8.01). In this case, there are one direction associated with non-normal growth and two with exponential growth. These examples suggest that to capture both normal and non-normal instabilities, we must choose

$$r \geq \max\left(\dim \mathcal{E}_u, \dim \mathcal{E}_u^s\right), \tag{3.21}$$

where we emphasize that $\mathcal{E}_u$ and $\mathcal{E}_u^s$ pertain to the *full-order* operators. The above criterion is necessary and sufficient, provided that the OTD subspace is not orthogonal to $\mathcal{E}_u$ and $\mathcal{E}_u^s$.

In light of this, it should be clear that the choice of r should not be dictated solely by the number of unstable eigenvalues of the symmetric operator $(\mathbf{L}_e + \mathbf{L}_e^\intercal)/2$, despite what the criterion (3.11) used in the control law might suggest. In fact, the two issues are not related, since the criterion (3.11) appears *after* the order reduction step, so it operates using information about the reduced-order system only. As discussed in Sect. 3.2, we could adopt any scheme of our liking to control the reduced system (3.9). We chose to focus on the eigenvalues of the symmetric part of the reduced operator because it is relatively straightforward, and more importantly because in our quest to suppress non-normal instabilities such criterion is much more stringent than one based on the eigenvalues of the reduced operator, as evidenced by the following theorem.

Theorem 2 *Let $\mathbf{Q} \in \mathbb{R}^{r\times r}$ be a steady operator acting in the reduced space. If all eigenvalues of $(\mathbf{Q} + \mathbf{Q}^\intercal)/2$ have negative real part, then so do all eigenvalues of $\mathbf{Q}$.*

Proof Suppose $\mathbf{Q}$ has at least one unstable eigenvalue. For a reduced-order dynamical system $\dot{\mathbf{x}} = \mathbf{Q}\mathbf{x}$ and a Lyapunov function $\mathbf{x}^\intercal\mathbf{x}$, the quadratic form $\mathbf{x}^\intercal(\mathbf{Q} + \mathbf{Q}^\intercal)\mathbf{x}$ describes the derivative of the Lyapunov function along trajectories. If $\mathbf{x}^\intercal(\mathbf{Q} + \mathbf{Q}^\intercal)\mathbf{x}$ is negative semi-definite, then the Euclidean norm of all trajectories is non-increasing. This contradicts the assumption that $\mathbf{Q}$ has at least one unstable eigenvalue. Thus, at least one eigenvalue of $(\mathbf{Q} + \mathbf{Q}^\intercal)/2$ is unstable. □

3.4.3 Validity of the control strategy

As discussed in Sect. 3.3, the final form of the control law (3.19) was derived on the basis of several key assumptions. We now discuss the extent to which these assumptions might restrict the scope of the proposed algorithm. First, the control law was designed to act on the variational equation (3.3), but we decided to apply it to the original nonlinear equation (3.1). This is valid as long as the norm of the perturbation $\mathbf{z} - \mathbf{z}_e$ is relatively small, so that the original dynamics may be described by the linearized equations. In (3.2), we also used the operator $\mathbf{L}(\mathbf{z})$ as a proxy for $\mathbf{L}_e$, which likewise holds

only when $\|\mathbf{z}-\mathbf{z}_e\|$ is small. This step was taken in an effort to guarantee consistency with the OTD framework, since the OTD modes are computed along an evolving trajectory, rather than at the fixed point. In doing so, we take full advantage of the fact that the OTD modes adaptively track directions of instability, rather than being "static" like eigenfunctions.

Second, by letting $\mathbf{B}=\mathbf{I}$, we assumed that the control can act on every state variable of the system, and the linearized system (3.3) is trivially controllable [45]. This is not a bad assumption to make in theory, but it rarely holds in experiments because the range and number of actuators are generally limited. Similarly, we have assumed complete knowledge of the state $\mathbf{z}$ of the system at every time instant, thereby implying full observability. While the assumption of full controllability may presumably be relaxed, we note that there is no avoiding the full observability assumption, simply because complete knowledge of the state is required to evolve the OTD equations (2.5). There is currently no general framework to compute or approximate the OTD modes with limited knowledge of the system state or the associated linearized operator.

The other assumptions, namely that the control vector belongs to the OTD subspace and the matrix $\mathbf{A}_r$ is symmetric, are deemed to be minor. The former was introduced to arrive at a relatively simple form of the control force without having to develop an entirely new theory to solve the control problem, and the latter was made to guarantee dynamical consistency of the order reduction. We note that a large part of feedback control theory focuses on pole placement for the linearized operator itself, and we are aware of no previous attempt made to find an optimal solution to the control problem in which the controller is designed to force the eigenvalues of the *symmetric part* of the linearized operator to the stable portion of the complex plane. A rigorous treatment of this problem could allow us to formulate a control law in which the two assumptions mentioned above would no longer be needed, but such endeavor is beyond the scope of the present work.

4 Results

In this section, we present evidence of the efficacy of the control strategy introduced in Sect. 3. We consider examples dominated by normal and non-normal instabilities and demonstrate the superiority of OTD control in situations exhibiting significant transient growth. In all that follows, we assume that the control is activated at $t=0$ and remains active for all $t>0$.

4.1 Suppression of normal instability by OTD control

For normal instability, the main advantage of OTD control over modal control is that it eliminates the need for computing the eigenfunctions of the linearized operator $\mathbf{L}_e$ beforehand, since asymptotically the OTD subspace aligns *by itself* with the most unstable eigenspace of $\mathbf{L}_e$. As discussed in Sect. 3.4.2, there is no gain related to the dimension of the projection subspace, because the dimension of the OTD control subspace must be at least as large as that of the unstable eigenspace. So for normal instability, and because we have assumed that the deviation $\mathbf{z}-\mathbf{z}_e$ remains small, we expect that a control based on the eigenmodes of $\mathbf{L}_e$ should be just as efficient as one based on OTD modes computed along the trajectory. (This may be viewed as a validation step.) We confirm that that is the case in two classical examples from fluid mechanics, namely flow past a cylinder and Kolmogorov flow.

4.1.1 Flow past a cylinder

We consider the two-dimensional flow of a Newtonian fluid with constant density ρ and kinematic viscosity ν past a circular cylinder of diameter D with uniform free-stream velocity $U\mathbf{e}_x$, for which the Navier–Stokes equations can be written in dimensionless form as

$$\partial_t\mathbf{w}+\mathbf{w}\cdot\nabla\mathbf{w}=-\nabla p+\frac{1}{Re}\nabla^2\mathbf{w}, \tag{4.1a}$$

$$\nabla\cdot\mathbf{w}=0, \tag{4.1b}$$

with no-slip boundary condition

$$\mathbf{w}|_{\Gamma_{\text{cyl}}}=\mathbf{0} \tag{4.2a}$$

on the cylinder surface Γ_{cyl}, and uniform flow

$$\lim_{x,y\to\infty}\mathbf{w}=\mathbf{e}_x \tag{4.2b}$$

in the far field. In the above, velocity, time, and length have been scaled with cylinder diameter D and free-stream velocity U, and the Reynolds number is $Re=UD/\nu$. The ith OTD mode obeys

$$\dot{\mathbf{u}}_i = \mathscr{L}_{NS}(\mathbf{w};\mathbf{u}_i) - \langle \mathscr{L}_{NS}(\mathbf{w};\mathbf{u}_i),\mathbf{u}_i\rangle\,\mathbf{u}_i - \sum_{k=1}^{i-1}\left[\langle \mathscr{L}_{NS}(\mathbf{w};\mathbf{u}_i),\mathbf{u}_k\rangle + \langle \mathscr{L}_{NS}(\mathbf{w};\mathbf{u}_k),\mathbf{u}_i\rangle\right]\mathbf{u}_k, \tag{4.3a}$$

$$\nabla\cdot\mathbf{u}_i = 0, \tag{4.3b}$$

with boundary conditions

$$\mathbf{u}_i|_{\Gamma_{\text{cyl}}} = \mathbf{0} \tag{4.4a}$$

and

$$\lim_{x,y\to\infty}\mathbf{u}_i = \mathbf{0}, \tag{4.4b}$$

where the inner product is chosen to be the usual L^2 inner product. The linearized Navier–Stokes operator at the current state $\mathbf{w}$ is given by

$$\mathscr{L}_{NS}(\mathbf{w};\mathbf{u}_i) = -\mathbf{w}\cdot\nabla\mathbf{u}_i - \mathbf{u}_i\cdot\nabla\mathbf{w} + \frac{1}{Re}\nabla^2\mathbf{u}_i - \nabla p_i, \tag{4.5}$$

where p_i is the pressure field that guarantees incompressibility of the OTD mode $\mathbf{u}_i$. The reduced linear operator is given by (3.7), with $\mathscr{L}_{NS}$ in place of $\mathscr{L}$.

The computational solution is effected using the open-source, spectral element Navier–Stokes solver `nek5000` [18]. The computational domain extends $24D$ cylinder diameters in the cross-stream direction and $32.4D$ in the streamwise direction, with the cylinder center located $8.4D$ away from the inlet boundary and equidistantly from the sidewalls. Our production runs use a mesh with 316 spectral elements, polynomial degree $N = 9$, and time-step size $\Delta\tau = 2\times10^{-3}$. We specify a no-penetration ("symmetry") boundary condition on the sidewalls and a stress-free condition at the outlet for the main flow and the OTD modes. At the inlet, we prescribe a non-homogeneous Dirichlet condition ($\mathbf{w} = \mathbf{e}_x$) for the main flow and a homogeneous Dirichlet condition for the OTD modes. Here and in what follows, we compute the OTD modes with $\mathbf{\Phi}$ given by (2.6), rather than $\mathbf{\Phi} = \mathbf{0}$, because the former allows use of the "standard approach" of Benettin et al. [7] and Shimada and Nagashima [42] in the limit of continuous orthonormalization (i.e., when the Gram–Schmidt procedure is applied at every time step). We refer the reader to Blanchard and Sapsis [8] for further details.

It is well known that for any value of Re, (4.1a, b–4.2a, b) admit a steady solution $\mathbf{w}_e$ symmetric about the midplane $y = 0$. The steady solution $\mathbf{w}_e$ loses stability at $Re_c \approx 47$ through a Hopf bifurcation resulting from a pair of complex conjugate eigenvalues crossing the imaginary axis. It has also been shown that in a range of Re values slightly above Re_c, there is exactly one pair of unstable complex conjugate eigenvalues [13,20]. Here, we consider the case $Re = 50$, which falls within that range, and for which the long-time attractor is a limit cycle. We compute the steady (unstable) base flow $\mathbf{w}_e$ by a selective frequency damping (SFD) approach [1], and the spectrum of $\mathscr{L}_{NS,e}$ by an Arnoldi algorithm [30]. Figure 1a–c shows the most unstable eigenvalues of $\mathscr{L}_{NS,e}$, along with the vorticity distribution of $\mathbf{w}_e$, and a snapshot of the vorticity

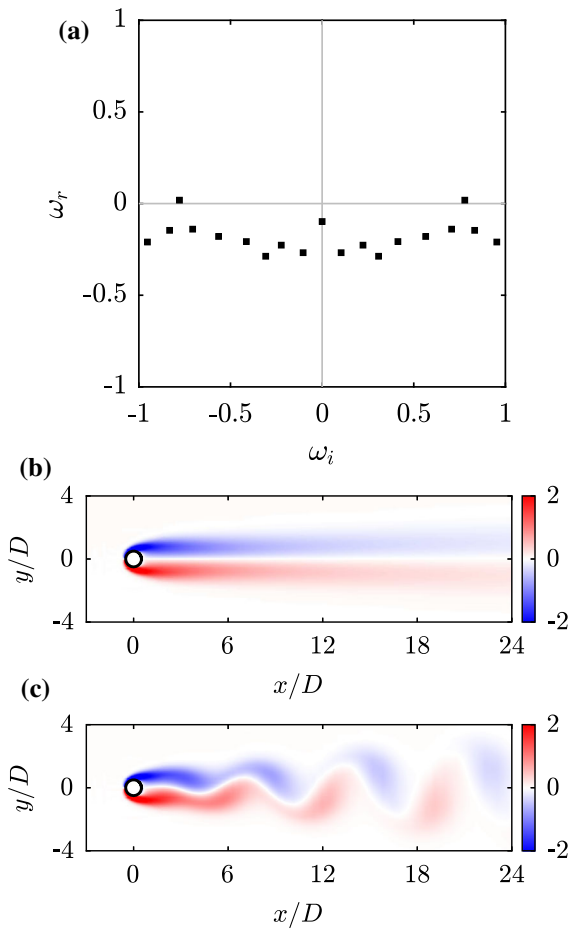

Fig. 1 For flow past a cylinder at $Re = 50$, **a** most unstable eigenvalues of the linear operator visualized in the complex plane, **b** spanwise vorticity distribution of the steady symmetric solution, and **c** snapshot of the spanwise vorticity distribution of the solution on the limit cycle in the absence of control

distribution of $\mathbf{w}$ on the limit cycle (in the absence of any control). Consistent with previous studies [30,40], Fig. 1a shows that there is only one pair of unstable complex conjugate eigenvalues, so we expect that a control based on two or more OTD modes should stabilize the steady symmetric solution.

We now use the OTD control law introduced in Sect. 3 to suppress linear instability of $\mathbf{w}_e$. We initialize the flow on the steady symmetric solution, to which we superimpose a small-amplitude inlet perturbation, so that

$$\mathbf{w}_{\text{inlet}}(y, t = 0) = \left(1 + 10^{-5} y\right) \mathbf{e}_x. \tag{4.6}$$

The condition that $\|\mathbf{w} - \mathbf{w}_e\|$ be small is thus satisfied at $t = 0$. To initialize the OTD modes, we apply Gram–Schmidt orthonormalization to the subspace $\{\sin(my)\mathbf{e}_x + \cos(mx)\mathbf{e}_y\}_{m=1}^{r}$. The resulting modes satisfy the divergence-free constraint. That they do not satisfy the boundary conditions is not an issue, because the OTD subspace aligns exponentially rapidly with $\mathcal{E}_u$ regardless of the initial conditions.

We first perform a computation with a single OTD mode. Figure 2a shows time series for the magnitude of the lift coefficient C_L and makes it clear that a control law based on one OTD mode cannot counteract linear instability of the steady flow. As discussed in Sect. 3, the reason is that order reduction of the linearized dynamics onto a one-dimensional OTD subspace leaves out the second linearly unstable direction. In contrast, Fig. 2b shows that a control law based on two OTD modes is able to stabilize $\mathbf{w}_e$. In Fig. 2b, we also introduced a stronger disturbance at $t = 600$, in the form of an inlet perturbation,

$$\mathbf{w}_{\text{inlet}}(y, t = 600) = \left(1 + 10^{-3} y\right) \mathbf{e}_x. \tag{4.7}$$

The amplitude of the inlet disturbance in (4.7) is small, yet two orders of magnitude larger than that imposed at $t = 0$. Figure 2b shows that the OTD control rapidly suppresses the imposed disturbance. We have verified that OTD subspaces with dimension larger than two lead to an identical outcome.

4.1.2 Kolmogorov flow

For a second example of normal instability, we consider Kolmogorov flow on the torus $\Omega = [0, 2\pi]^2$. The flow obeys the incompressible Navier–Stokes equations subject sinusoidal forcing, written in dimensionless form as

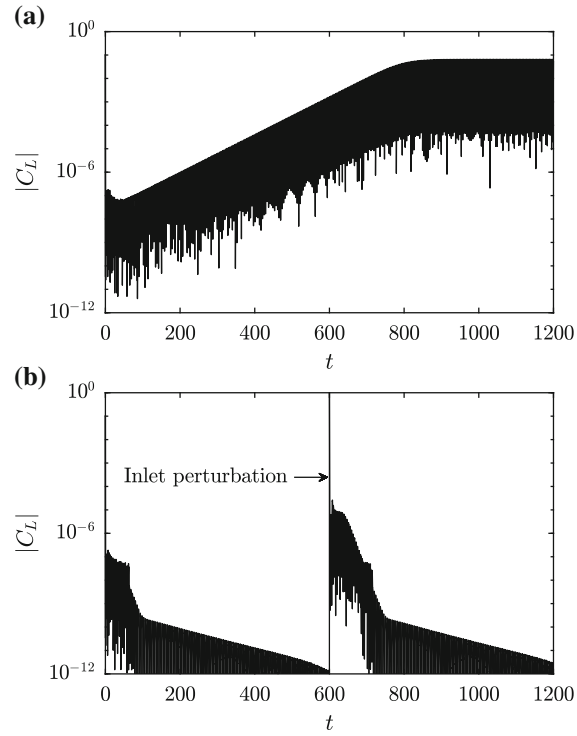

Fig. 2 For flow past a cylinder at $Re = 50$ with OTD control (with $\zeta = 0.1$), time series of $|C_L|$ for **a** $r = 1$, and **b** $r = 2$. In **b**, an inlet perturbation in the form of (4.7) is applied at $t = 600$

$$\partial_t \mathbf{w} + \mathbf{w} \cdot \nabla \mathbf{w} = -\nabla p + \frac{1}{Re} \nabla^2 \mathbf{w} + \sin(ky)\mathbf{e}_x, \tag{4.8a}$$

$$\nabla \cdot \mathbf{w} = 0, \tag{4.8b}$$

where k is a positive integer and the Reynolds number Re is the inverse of a dimensionless fluid viscosity ν. The OTD equations are identical to (4.3a, b), with $\mathscr{L}_{NS}$ given by (4.5). (We note that the external forcing does not appear in the expression for the linearized operator $\mathscr{L}_{NS}$.) The main flow and the OTD modes satisfy periodic conditions. The computational solution is effected using `nek5000` with a mesh composed of 256 elements (16 elements in each direction), polynomial order $N = 5$, and time-step size $\Delta t = 10^{-3}$.

The Kolmogorov flow admits a laminar solution,

$$\mathbf{w}_e = \frac{Re}{k^2} \sin(ky)\mathbf{e}_x, \tag{4.9}$$

which is asymptotically stable for forcing wave number $k = 1$ and any value of Re [19]. For $k > 1$ and large enough Re values, the laminar solution $\mathbf{w}_e$ is unstable. As discussed in Platt et al. [32] and Chandler and Kerswell [10], it is believed that for $k = 4$ and sufficiently

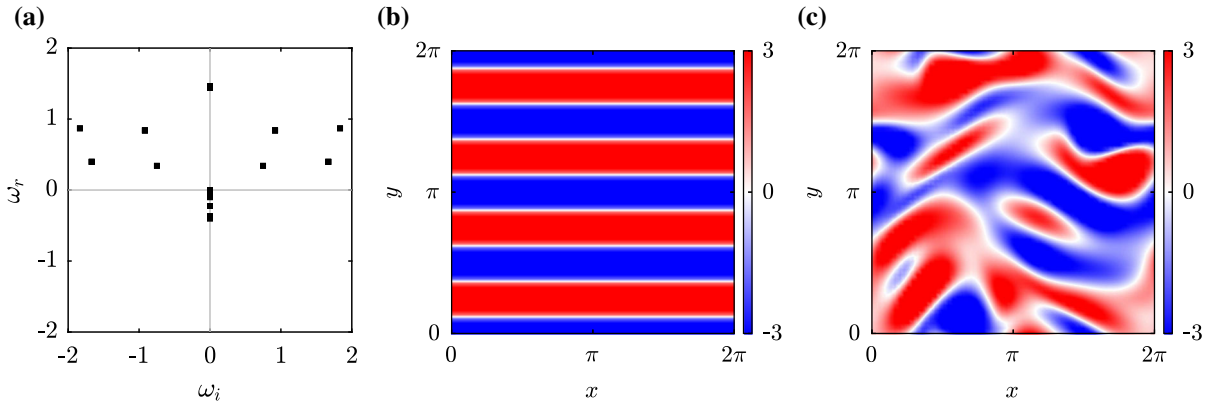

Fig. 3 For Kolmogorov flow with $Re = 40$ and $k = 4$, **a** 50 most unstable eigenvalues of the linear operator visualized in the complex plane, **b** spanwise vorticity distribution of the laminar solution, and **c** snapshot of the spanwise vorticity distribution of the solution in the chaotic regime in the absence of control

large Re, all fixed points of the Kolmogorov flow are unstable, and the long-time solution is chaotic. We note that other invariant solutions besides (4.9) are known to exist for this flow. For $k = 4$ and $Re = 40$, Farazmand [15] reported no fewer than 16 different steady (unstable) solutions, with dim $\mathcal{E}_u$ ranging from 5 to 38. Here, we use OTD control to stabilize the laminar solution (4.9), for which an analytical expression is available. We emphasize that OTD control may be used to stabilize *any* of the 16 solutions found by Farazmand [15], provided that the dimension of the OTD subspace is chosen according to (3.21).

In what follows, we set $k = 4$ and $Re = 40$, along the lines of Farazmand and Sapsis [16]. We first determine the dimension of the unstable eigenspace for the laminar solution (4.9). An Arnoldi calculation shows that dim $\mathcal{E}_u = 38$, consistent with Farazmand [15]. Figure 3a–c shows the 50 most unstable eigenvalues of $\mathbf{L}_e$, along with vorticity distributions of the laminar solution, and a snapshot of the solution in the chaotic regime (in the absence of feedback control). The Arnoldi algorithm reveals that among the 19 pairs of unstable complex conjugate eigenvalues, only 3 have multiplicity one (Fig. 3a). There is a possibility that such a high multiplicity might affect the rate at which alignment of the OTD subspace with $\mathcal{E}_u$ takes place, as the convergence result established by Babaee et al. [3] holds when there is a spectral gap between the rth and $(r+1)$th most unstable eigenvalues of $\mathbf{L}_e$. Fortunately, criterion (3.21) guarantees that the spectral gap assumption holds, so multiplicity will not be an issue in the cases considered hereinafter.

We perform two computations in which the control is active, one with $r = 36$ and the other with $r = 38$. For the case $r = 36$, we expect to see growth of the solution, as one pair of unstable eigenvalues is left out by the OTD order reduction and therefore not acted upon by the control. For the case $r = 38$, however, the dimension of the OTD subspace satisfies (3.21), so the feedback control should be able to stabilize the laminar solution. In both computations, the initial condition for the main flow is $\mathbf{w}(t = 0) = \mathbf{w}_e$, so linear instability is triggered by numerical noise. (A calculation without control shows that this mechanism is available.) Noise-induced disturbances may be considered infinitesimal, so the condition that $\|\mathbf{w} - \mathbf{w}_e\|$ be small is trivially satisfied at $t = 0$. To initialize the OTD modes, we apply Gram–Schmidt orthonormalization to the subspace $\{\cos(mx)\sin(my)\mathbf{e}_x - \sin(mx)\cos(my)\mathbf{e}_y\}_{m=1}^{r}$. The resulting modes thus satisfy the divergence-free constraint and the periodic boundary conditions.

Figure 4 shows time series for the energy dissipation

$$E_d(t) = \frac{1}{Re|\Omega|}\int_\Omega |\nabla \mathbf{w}|^2 \mathrm{d}\Omega \tag{4.10}$$

for the uncontrolled and the two controlled cases. When no control is applied, the trajectory rapidly leaves the vicinity of the laminar solution $\mathbf{w}_e$ (for which $E_d = 1.25$) as a result of linear instability and, after a brief transient regime, settles into a chaotic attractor. Figure 4 also shows that with a 36-dimensional OTD subspace, the control cannot do better than to delay repeal of the trajectory from $\mathbf{w}_e$. With a 38-dimensional OTD

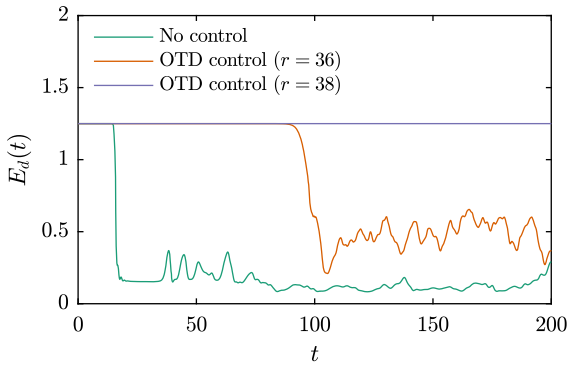

Fig. 4 Energy dissipation for trajectories with OTD control (with $\zeta = 0.1$) and without control. For the case with OTD control and $r = 38$, the calculation was terminated at $t = 2000$ to ascertain stability

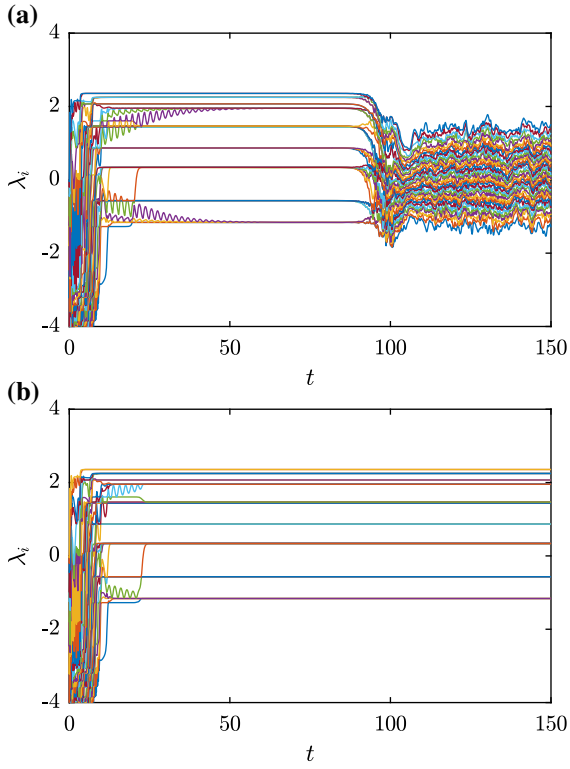

Fig. 5 Eigenvalues of the symmetric part of the open-loop reduced linear operator for the OTD-controlled trajectories shown in Fig. 4: **a** $r = 36$ and **b** $r = 38$

subspace, however, the control is able to suppress linear instability and stabilize the fixed point.

Figure 5a, b shows the eigenvalues of the symmetric part of the open-loop reduced linear operator for $r = 36$ and 38. In both cases, the OTD subspace aligns with the most unstable eigenspace of $\mathbf{L}_e$ quite rapidly (in about 10 time units), despite the fact that a large number of eigenvalues have multiplicity greater than one. The plateau beginning after alignment corresponds to a state in which the solution is infinitesimally close to the fixed point, and the OTD subspace is aligned with the most unstable eigenspace of $\mathbf{L}_e$. But it is only for $r = 38$, when all of the 38 unstable eigendirections of $\mathbf{L}_e$ are accounted for in the reduced-order system, that the control is able to suppress linear instability and exponential growth.

4.2 Suppression of non-normal instability by OTD control

As discussed in Sect. 2, the great value of the OTD framework has to do with control of instabilities caused by non-normal behavior. The OTD modes have a significant advantage over eigenfunctions, as the latter are not able to capture non-normal growth. While in Sect. 4.1 we took advantage of the asymptotic behavior of the OTD subspace (it coincides with the most unstable eigenspace) to suppress normal instabilities, here we wish to leverage their ability to track directions of greater transient growth along a trajectory. So to demonstrate the superiority of OTD control over modal control, we focus primarily on situations in which the fixed point is linearly (asymptotically) stable, but significant growth of the solution occurs as a result of transient non-normal instability.

Comparison of OTD and modal control is only fair if the same control law is used in both approaches. To apply (3.19) to modal control, we proceed as follows. From the leading r eigenvectors of $\mathbf{L}_e$, we construct an orthonormal basis $\boldsymbol{\psi}$ using the Gram–Schmidt algorithm. We then use $\boldsymbol{\psi}$ in lieu of the OTD modes $\mathbf{U}$. Furthermore, we consider the reduced linear operator $\boldsymbol{\psi}^\mathsf{T}\mathbf{L}_e\boldsymbol{\psi}$, rather than $\boldsymbol{\psi}^\mathsf{T}\mathbf{L}\boldsymbol{\psi}$. Since the concept of eigenvectors is fundamentally tied to that of a fixed point, we argue that projecting $\mathbf{L}_e$ on $\boldsymbol{\psi}$ is the only sensible option. It makes little sense to consider situations in which $\mathbf{L}$ is projected onto an eigenspace of $\mathbf{L}$, because eigenvectors of a time-dependent operator are meaningless. The remaining variations (projecting $\mathbf{L}_e$ on an eigenspace of $\mathbf{L}$, and vice versa) are inconsistent for the same reason. In contrast, the OTD modes are computed along time-dependent trajectories, and the projection of $\mathbf{L}$ on an OTD subspace is dynamically

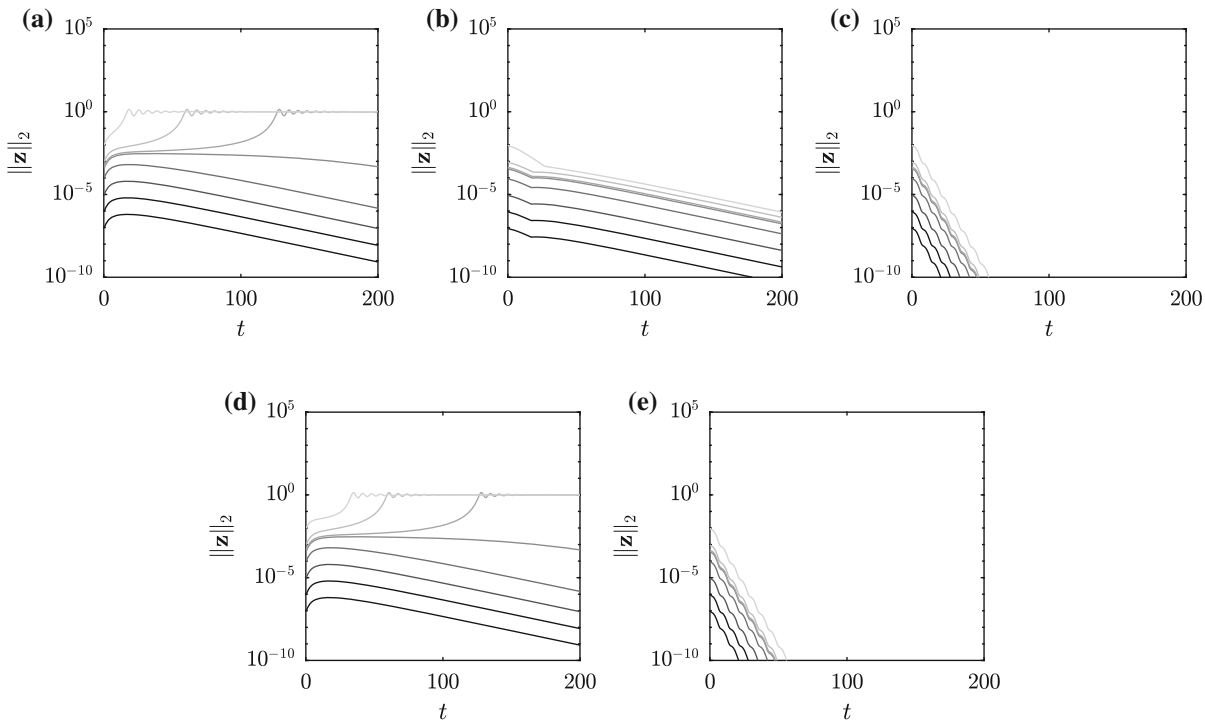

Fig. 6 For the 2×2 non-normal system (4.11a, b), norm of trajectories subject to **a** no control, **b** OTD control with $r = 1$, **c** OTD control with $r = 2$, **d** modal control based on the most unstable eigenvector of $\mathbf{C}$, and **e** modal control based on the two eigenvectors of $\mathbf{C}$. Initial conditions for the trajectories are $(0, c)^\intercal$, where $c = 10^{-7}, 10^{-6}, 10^{-5}, 10^{-4}, 4 \times 10^{-4}, 5 \times 10^{-4}, 10^{-3}, 10^{-2}$, from darker to lighter

consistent and meaningful. (For an uncontrolled trajectory exhibiting significant non-normal growth, the OTD subspace significantly departs from the most unstable eigenspace $\mathbf{L}_e$). Finally, we use the same value of the damping parameter ζ for OTD and modal control.

4.2.1 Unsteady low-dimensional nonlinear system

As discussed in Sect. 1, a critical application of OTD control to non-normal systems is to prevent transition to turbulence. So we begin with a simple low-dimensional nonlinear problem introduced by Trefethen et al. [46],

$$\dot{\mathbf{z}} = \mathbf{C}\mathbf{z} + \|\mathbf{z}\|\mathbf{D}\mathbf{z}, \tag{4.11a}$$

where

$$\mathbf{C} = \begin{bmatrix} -1/R & 1 \\ 0 & -2/R \end{bmatrix}, \quad \mathbf{D} = \begin{bmatrix} 0 & -1 \\ 1 & 0 \end{bmatrix}, \tag{4.11b}$$

and R is a large parameter (here, $R = 25$). The linear term involving the non-normal matrix $\mathbf{C}$ amplifies energy transiently, while the nonlinear term involving the skew-symmetric matrix $\mathbf{D}$ redistributes, but neither creates nor destroy, energy. A remarkable feature of this system is that, despite the fact that the trivial fixed point $\mathbf{z}_e = \mathbf{0}$ is asymptotically stable (the eigenvalues of $\mathbf{C}$ are negative), it is possible for a perturbation to be sufficiently amplified that it activates the nonlinear terms, leading to transition to "turbulence." This particular behavior (non-normal amplification coupled with energy-preserving nonlinear mixing) is common in fluid mechanics, which makes this system a good testbed for our control algorithm. We illustrate the potential of this system in Fig. 6a, where we show the norm of uncontrolled trajectories integrated forward in time with initial condition $(0, c)^\intercal$, where c is a constant. (Integration is performed with a third-order Adams–Bashforth method with time-step size $\Delta t = 0.1$.) Figure 6a makes it clear that large enough non-normal growth leads to transition to "turbulence." (For this simple 2×2 system, the long-time "turbulent" attractor is actually another fixed point.)

Here, the mechanism responsible for transient growth is well understood. The culprit is the principal right singular vector of $\mathbf{C}$, as it finds itself on the receiving end of a self-sustained transfer of energy facilitated by the nonlinear terms. Thus, there is only one direction responsible for non-normal growth, and that direction coincides with neither of the eigenvectors of $\mathbf{C}$. So modal control should work only when all the eigenvectors of $\mathbf{C}$ are included in the control space, since neither of them can individually track the direction of non-normal growth. On the other hand, OTD control with $r = 1$ should be able to suppress non-normal growth and, in turn, prevent transition to "turbulence." This is confirmed in Fig. 6b–e. (In Fig. 6b, c, initial conditions for the OTD modes are selected randomly.)

4.2.2 Plane Poiseuille flow

There is no geometry simpler than that of plane Poiseuille flow to study the effects of non-normality in the Navier–Stokes equations. Plane Poiseuille flow consists of pressure-driven flow confined between two rigid, infinitely long, parallel plates. The Navier–Stokes equations can be written in dimensionless form as

$$\partial_t \mathbf{w} + \mathbf{w} \cdot \nabla \mathbf{w} = -\nabla p + \frac{1}{Re}\nabla^2 \mathbf{w} + \frac{2}{Re}, \tag{4.12a}$$

$$\nabla \cdot \mathbf{w} = 0, \tag{4.12b}$$

with boundary conditions

$$\mathbf{w}(x, y = \pm 1, z, t) = \mathbf{0} \tag{4.12c}$$

at the rigid walls. Velocity, time, and length have been scaled with the channel half-width h and the centerline velocity U of the undisturbed flow. The Reynolds number is $Re = Uh/\nu$, where ν is the kinematic viscosity of the fluid. The undisturbed base flow

$$\mathbf{w}_e(x, y, z) = W(y)\mathbf{e}_x, \quad W(y) = 1 - y^2 \tag{4.13}$$

is a fixed point of (4.12a–c) and is known to become linearly unstable at $Re_c \approx 5772.2$. However, experiments suggest another value for Re_c (on the order of 1000), drastically different from that predicted by modal stability analysis. This is due to the strongly non-normal nature of the dynamics, whereby perturbations may experience significant transient growth, even in the spectrally stable regime. For sufficiently small perturbations, this transient growth does not persist at long times, and the system asymptotically returns to the laminar solution. For sufficiently strong perturbations, however, non-normal growth is so large that the path to steadiness is blocked by nonlinear effects, ultimately leading to turbulence by triggering secondary three-dimensional instabilities.

We first consider the linearized dynamics of infinitesimal perturbations around the base flow (4.13). Because of the infinite extent of the domain in the x and z directions, the infinitesimal disturbance is assumed to have the form

$$\mathbf{q}'(x, y, z, t) = \mathbf{q}(y, t)\exp(i\alpha x + i\beta z), \tag{4.14}$$

where α and β denote the streamwise and spanwise wavenumbers, respectively, and the vectors $\mathbf{q}$ and $\mathbf{q}'$ contain the wall-normal velocity (v and v', respectively) and the wall-normal vorticity (η and η', respectively) in lieu of the primitive variables [40]. This leads to the classical Orr–Sommerfeld/Squire (OS/SQ) equation

$$\partial_t \mathbf{q} = \mathscr{L}_e(\mathbf{q}), \tag{4.15}$$

with boundary conditions $v = \mathscr{D}(v) = \eta = 0$ at the rigid walls $y = \pm 1$, where

$$\mathscr{L}_e = \begin{bmatrix} \mathscr{L}_{OS} & 0 \\ \mathscr{L}_C & \mathscr{L}_{SQ} \end{bmatrix}, \tag{4.16a}$$

$$\mathscr{L}_{OS} = -\left(k^2 - \mathscr{D}^2\right)^{-1}\left[i\alpha W(k^2 - \mathscr{D}^2) + i\alpha\mathscr{D}^2(W) + \frac{1}{Re}\left(k^2 - \mathscr{D}^2\right)^2\right], \tag{4.16b}$$

$$\mathscr{L}_C = -i\beta\mathscr{D}(W), \tag{4.16c}$$

$$\mathscr{L}_{SQ} = -i\alpha W - \frac{1}{Re}\left(k^2 - \mathscr{D}^2\right), \tag{4.16d}$$

and we have defined $\mathscr{D} = \partial_y$ and $k = \sqrt{\alpha^2 + \beta^2}$. (For further details regarding the derivation of the OS/SQ, we refer the reader to Schmid and Brandt [40]). The OTD equations are identical to (2.7), with $\mathscr{L}$ substituted for $\mathscr{L}_e$ as defined in (4.16a–d). The natural choice for the inner product is the energy inner product, defined as

$$\langle \mathbf{q}_1, \mathbf{q}_2 \rangle_E = \int_{-1}^{1} \mathbf{q}_1^{\mathsf{T}} \mathscr{M}(\mathbf{q}_2)\mathrm{d}y, \tag{4.17}$$

where

$$\mathscr{M} = \frac{1}{k^2}\begin{bmatrix} \left(k^2 - \mathscr{D}^2\right) & 0 \\ 0 & 1 \end{bmatrix}. \tag{4.18}$$

We emphasize that for now, we only consider the evolution of perturbations described by (4.15), so the dynamics are linear, and the operator $\mathscr{L}_e$ used in the

OTD equations is steady. (The full nonlinear initial-boundary-value problem (4.12a–c) will be considered shortly). Equation (4.15) is discretized in space using a spectral method based on Chebyshev polynomials and integrated forward in time with a third-order backward differentiation (BDF) scheme. We use 128 collocation points in space and a time-step size of $\Delta t = 0.02$.

We pause here to make several comments on the OS/SQ operator and the various flow regimes that it may lead to as a function of the Reynolds number. For two-dimensional waves propagating in the streamwise direction ($\beta = 0$), three regimes may be identified. For $Re < 49.6$, the OS/SQ operator is normal and asymptotically stable, so the amplitude of perturbations monotonically decays. For $49.6 < Re < 5772.2$, the OS/SQ operator is non-normal and asymptotically stable, so perturbations experience significant transient growth before dying out. For $Re > 5772.2$, the OS/SQ operator is non-normal and asymptotically unstable, so transient growth of perturbations is followed by exponential growth. To make this point visually clear, Fig. 7a shows time series of the optimal energy amplification

$$G(t) = \max_{\mathbf{q}_0} \frac{\|\mathbf{q}(t)\|_E^2}{\|\mathbf{q}_0\|_E^2} \tag{4.19}$$

for $\beta = 0$ and $\alpha = 1.02$ (the most unstable streamwise wavenumber for $\beta = 0$). For $Re = 2000$, it is clear that substantial transient growth occurs, with perturbation energy growing by more than one order of magnitude, despite the fact that all the eigenvalues of the OS/SQ operator are confined to the stable portion of the complex plane (Fig. 7b).

We are now in a position to apply the control strategy described in Sect. 3 to the linear OS/SQ problem (4.15). We consider streamwise and spanwise wavenumbers $\alpha = 1.02$ and $\beta = 0$, respectively, and two values of the Reynolds number, $Re = 2000$ and 10,000 (cf. Fig. 7a). The former Re value is such that in the OS/SQ linearized dynamics, non-normal growth is followed by exponential decay, so transition to turbulence would occur in direct numerical simulations (DNS) of the full nonlinear problem (4.12a–c) only if the energy of the perturbation is sufficiently amplified. The latter Re value is such that in the OS/SQ linearized dynamics, non-normal growth is followed by exponential (asymptotic) growth, so transition to turbulence would invariably occur in DNS of the nonlinear initial-boundary-value problem.

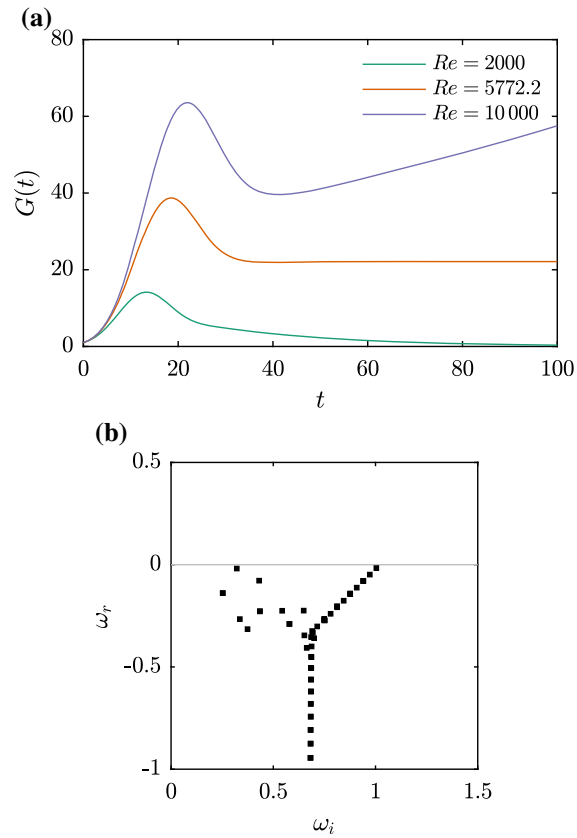

Fig. 7 For linearized plane Poiseuille flow with $\alpha = 1.02$ and $\beta = 0$, **a** optimal energy amplification, and **b** spectrum of the OS/SQ operator at $Re = 2000$

The initial condition for (4.15) is taken to be the *optimal initial condition*

$$\mathbf{q}_0^{\text{opt}} = \operatorname*{argmax}_{\mathbf{q}_0} \frac{\|\mathbf{q}(t^*)\|_E^2}{\|\mathbf{q}_0\|_E^2} \tag{4.20}$$

that leads to maximal transient growth over the time interval $[0, t^*]$, where t^* is the time at which maximum energy amplification over all initial conditions is attained. Figure 7a shows that $t^* \approx 13.3$ for $Re = 2000$ and $t^* \approx 21.9$ for $Re = 10{,}000$. (In the latter case, we consider only the transient portion of the time series, since exponential growth necessarily means $t^* = +\infty$.) As discussed in Schmid and Brandt [40], the optimal initial condition $\mathbf{q}_0^{\text{opt}}$ is the leading right singular vector of the propagator $\exp(\mathbf{L}_e t^*)$. The OTD modes are initialized against the leading r right singular vectors of $\exp(\mathbf{L}_e t^*)$. We note that due to the strongly non-normal nature of $\mathbf{L}_e$ at $Re = 2000$ and

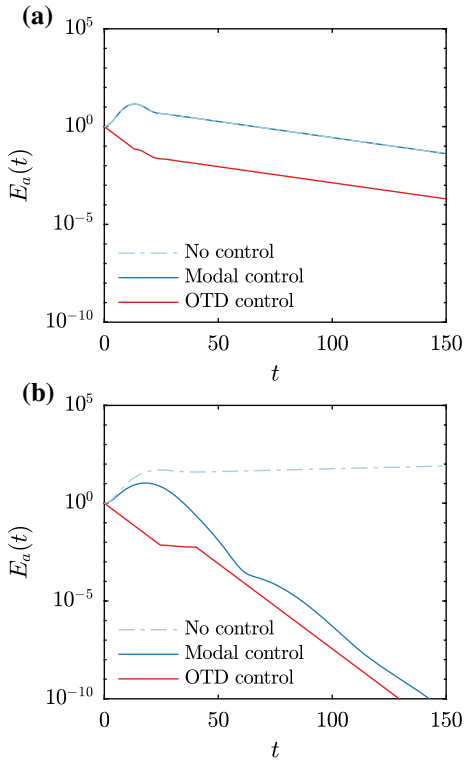

Fig. 8 For linearized plane Poiseuille flow with $\alpha = 1.02$ and $\beta = 0$, energy amplification of the optimal perturbation with OTD control ($r = 1$ and $\zeta = 0.1$), modal control based on the most unstable eigenvector of the OS/SQ operator, and no control, for **a** $Re = 2000$, and **b** $Re = 10{,}000$

10,000, a large number of eigenvectors are required to accurately represent the optimal condition.

Figure 8a, b shows time series for the energy amplification

$$E_a(t) = \frac{\|\mathbf{q}(t)\|_E^2}{\|\mathbf{q}_0\|_E^2} \tag{4.21}$$

of $\mathbf{q}_0^{\text{opt}}$ with and without modal and OTD control at $Re = 2000$ and 10,000. In all cases, there is only one direction associated with transient growth (that of $\mathbf{q}_0^{\text{opt}}$). Figure 8a shows that OTD control with a single OTD mode is able to suppress non-normal growth of $\mathbf{q}_0^{\text{opt}}$ for $Re = 2000$ and 10,000. For $Re = 10{,}000$, OTD control also suppresses normal instability and prevents exponential growth at long times. On the other hand, Fig. 8a, b shows that modal control with one eigenvector (here, the most unstable one) does not suppress non-normal growth at $Re = 2000$ and 10,000, although for $Re = 10{,}000$ it is able to eliminate asymptotic exponential growth. (There is only one unstable eigenvalue at $Re = 10{,}000$.)

As discussed earlier, transient growth may have severe repercussions on the long-time dynamics, even in cases where modal stability theory predicts asymptotic decay of disturbances. For a clear manifestation of this mechanism, we must consider the full nonlinear problem (4.12a–c), which we solve numerically using `nek5000` in a computational domain extending $2\pi/\alpha$ and $2\pi/\beta$ in the streamwise and spanwise directions, respectively. The mesh is composed of 96 elements with polynomial order $N = 9$, and the time-step size is $\Delta t = 4 \times 10^{-3}$. The main flow and the OTD modes satisfy no-slip boundary conditions on the rigid walls and periodic boundary conditions in the x and z directions. The OTD equations are given by (4.3a, b), where the linear operator is identical to (4.5). We emphasize that the linear operator appearing in the OTD equations is now unsteady and computed along the evolving trajectory.

For three-dimensional turbulence to develop, the spanwise wavenumber β should not be zero, so we choose $\beta = 2$, along with $\alpha = 0.5$ and $Re = 7000$. For these values of the parameters, linear theory predicts significant non-normal growth of the optimal initial condition (on the order of 1000), followed by asymptotic decay. However, in the full nonlinear problem, sufficiently large non-normal growth triggers transition to turbulence. To confirm that this mechanism is available in our numerical experiments, we select initial conditions for the main flow as

$$\mathbf{w}(x, y, z, t = 0) = \mathbf{w}_e(x, y, z) + \varepsilon \mathbf{w}_0^{\text{opt}}(x, y, z), \tag{4.22}$$

where the parameter ε governs the strength of the initial disturbance. (We compute $\mathbf{w}_0^{\text{opt}}$ by expressing $\mathbf{q}_0^{\text{opt}}$ in terms of the primitive variables.) Figure 9a shows that transient growth occurs for a range of ε values, but ultimately leads to turbulence only when ε is large enough. As discussed in Sect. 4.2.1, the physical mechanism for transition is that sufficiently large energy amplification activates the nonlinearity of the Navier–Stokes equations, which in turn redistributes energy to directions associated with transient growth.

We apply our OTD control strategy to the full nonlinear system in an attempt to suppress transition to turbulence. As in the linearized problem, we consider a control based on a single OTD mode initialized in the direction of the optimal disturbance $\mathbf{w}_0^{\text{opt}}$. Figure 9b

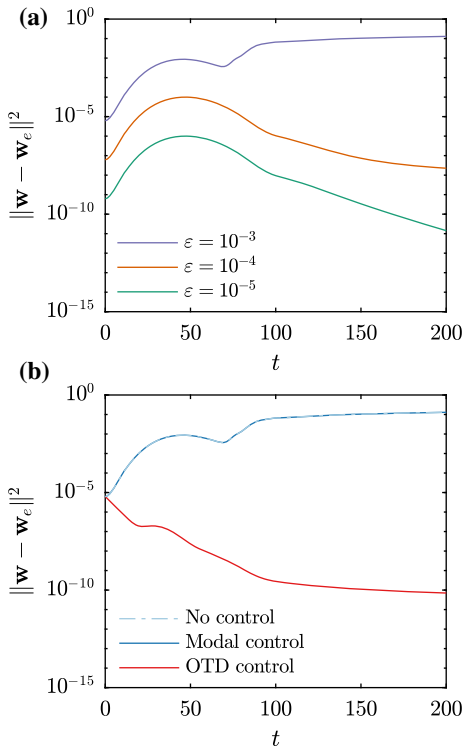

Fig. 9 For nonlinear plane Poiseuille flow with $\alpha = 0.5$, $\beta = 2$, and $Re = 7000$, **a** energy of uncontrolled perturbation for various disturbance amplitudes, and **b** for $\varepsilon = 10^{-3}$, energy of perturbation with OTD control ($r = 1$ and $\zeta = 0.1$), modal control based on the most unstable eigenvector of the OS/SQ operator, and no control

shows that OTD control suppresses non-normal growth and, in turn, transition to turbulence. In contrast, modal control based on the most unstable eigenvector of $\mathbf{L}_e$ fails at both. This completes demonstration of the superiority of OTD control over modal control.

5 Conclusions

The purpose of the present work was to develop a reduced-order control algorithm capable of suppressing transient and long-time linear instabilities of a fixed point for a generic (high-dimensional, nonlinear) dynamical system. The challenge was to find an appropriate set of complete functions (i.e., modes) such that projection of the governing equations onto these modes retained the critical features of the full-order dynamics related to transient and asymptotic instabilities as the system evolves in phase space. The optimally time-dependent (OTD) modes presented themselves as a natural candidate for order reduction because they had been shown to adaptively capture and track directions in phase space associated with transient and persistent instabilities.

We used OTD modes to derive a dynamically consistent reduced-order system and formulated a control law in the reduced space that targets instantaneous growth of perturbations in order to suppress transient and asymptotic instabilities of a fixed point of the full-order governing equations. We derived conditions on the OTD subspace for the control to be efficient and applied the proposed strategy to complex fluid flows exhibiting normal (exponential) and non-normal (transient) growth. For systems featuring normal instabilities, we showed that our control strategy reduces to classical modal control, as the OTD subspace aligns asymptotically with the most unstable eigenspace of the linearized operator. For systems with non-normal instabilities, however, we showed that OTD control vastly outperforms modal control, as the OTD modes are able to track directions of most intense transient growth, which is far beyond the reach of eigenfunctions. This result was significant because it established the potential of the OTD framework to prevent regime transitions caused by non-normal growth, such as transition to turbulence in fluid flows.

Finally, we mention two ways in which the proposed control strategy may be improved. First, it would be desirable to design a feedback control law that acts only in part of the physical domain, say, a confined area in the near wake for flow past a cylinder, or the immediate vicinity of the rigid walls for Poiseuille flow. This would make the proposed approach considerably more attractive from the standpoint of conducting experiments. Second, along the same lines, it would be valuable to make the OTD control approach data-driven; for example, formulate a method for computing the OTD modes from sparse measurement data or develop a machine learning algorithm that help identify and control transient instabilities in complex flows.

Acknowledgements The authors gratefully acknowledge insightful discussions with Dr. Mohammad Farazmand.

Funding This study was supported by Army Research Office Grant W911NF-17-1-0306 and Air Force Office of Scientific Research Grant FA9550-16-1-0231.

Compliance with ethical standards

Conflict of interest The authors declare that they have no conflict of interest.

References

1. Åkervik, E., Brandt, L., Henningson, D.S., Hœpffner, J., Marxen, O., Schlatter, P.: Steady solutions of the Navier–Stokes equations by selective frequency damping. Phys. Fluids **18**, 068102 (2006)
2. Åström, K.J., Kumar, P.R.: Control: a perspective. Automatica **50**, 3–43 (2014)
3. Babaee, H., Farazmand, M., Haller, G., Sapsis, T.P.: Reduced-order description of transient instabilities and computation of finite-time Lyapunov exponents. Chaos Interdiscip. J. Nonlinear Sci. **27**, 063103 (2017)
4. Babaee, H., Sapsis, T.P.: A minimization principle for the description of modes associated with finite-time instabilities. Proc. R. Soc. A **472**, 20150779 (2016)
5. Balasubramanian, K., Sujith, R.I.: Thermoacoustic instability in a Rijke tube: non-normality and nonlinearity. Phys. Fluids **20**, 044103 (2008)
6. Bayly, B.J.: Three-dimensional instability of elliptical flow. Phys. Rev. Lett. **57**, 2160 (1986)
7. Benettin, G., Galgani, L., Strelcyn, J.M.: Kolmogorov entropy and numerical experiments. Phys. Rev. A **14**, 2338 (1976)
8. Blanchard, A., Sapsis, T.P.: Analytical description of optimally time-dependent modes for reduced-order modeling of transient instabilities (2018) (Submitted to SIAM Journal on Applied Dynamical Systems)
9. Blanchard, A., Sapsis, T.P.: Stabilization of unsteady flows by reduced-order control with optimally time-dependent modes (2018) (Submitted to Physical Review Fluids)
10. Chandler, G.J., Kerswell, R.R.: Invariant recurrent solutions embedded in a turbulent two-dimensional Kolmogorov flow. J. Fluid Mech. **722**, 554–595 (2013)
11. Chomaz, J.M.: Global instabilities in spatially developing flows: non-normality and nonlinearity. Annu. Rev. Fluid Mech. **37**, 357–392 (2005)
12. Duriez, T., Brunton, S.L., Noack, B.R.: Machine Learning Control: Taming Nonlinear Dynamics and Turbulence. Springer, Berlin (2017)
13. Dušek, J., Le Gal, P., Fraunié, P.: A numerical and theoretical study of the first Hopf bifurcation in a cylinder wake. J. Fluid Mech. **264**, 59–80 (1994)
14. Eisenman, I.: Non-normal effects on salt finger growth. J. Phys. Oceanogr. **35**, 616–627 (2005)
15. Farazmand, M.: An adjoint-based approach for finding invariant solutions of Navier–Stokes equations. J. Fluid Mech. **795**, 278–312 (2016)
16. Farazmand, M., Sapsis, T.P.: Dynamical indicators for the prediction of bursting phenomena in high-dimensional systems. Phys. Rev. E **94**, 032212 (2016)
17. Farrell, B.: Optimal excitation of neutral Rossby waves. J. Atmos. Sci. **45**, 163–172 (1988)
18. Fischer, P.F., Lottes, J.W., Kerkemeier, S.G.: `nek5000` Web page (2008). http://nek5000.mcs.anl.gov
19. Foias, C., Manley, O., Rosa, R., Temam, R.: Navier–Stokes Equations and Turbulence. Cambridge University Press, Cambridge (2001)
20. Giannetti, F., Luchini, P.: Structural sensitivity of the first instability of the cylinder wake. J. Fluid Mech. **581**, 167–197 (2007)
21. Guckenheimer, J., Holmes, P.: Nonlinear Oscillations, Dynamical Systems, and Bifurcations of Vector Fields. Springer, Berlin (1983)
22. Holmes, P., Lumley, J.L., Berkooz, G.: Turbulence, Coherent Structures, Dynamical Systems and Symmetry. Cambridge University Press, Cambridge (1998)
23. Juang, J.N., Pappa, R.S.: An eigensystem realization algorithm for modal parameter identification and model reduction. J. Guid. Control Dyn. **8**, 620–627 (1985)
24. Lumley, J.L.: Coherent structures in turbulence. In: Meyer, R.E. (ed.) Transition and Turbulence, pp. 215–242. Academic Press, New York (1981)
25. Mack, L.M.: The inviscid stability of the compressible laminar boundary layer. Space Prog. Summ. **37**, 297–312 (1963)
26. Moore, B.: Principal component analysis in linear systems: controllability, observability, and model reduction. IEEE Trans. Autom. Control **26**, 17–32 (1981)
27. Orszag, S.A.: Accurate solution of the Orr–Sommerfeld stability equation. J. Fluid Mech. **50**, 689–703 (1971)
28. Orszag, S.A., Patera, A.T.: Secondary instability of wall-bounded shear flows. J. Fluid Mech. **128**, 347–385 (1983)
29. Penland, C., Sardeshmukh, P.D.: The optimal growth of tropical sea surface temperature anomalies. J. Clim. **8**, 1999–2024 (1995)
30. Peplinski, A., Schlatter, P., Fischer, P.F., Henningson, D.S.: Stability tools for the spectral-element code Nek5000: application to jet-in-crossflow. In: Azaïez, M., El Fekih, H., Hesthaven, J.S. (eds.) Spectral and High Order Methods for Partial Differential Equations, pp. 349–359. Springer, Berlin (2014)
31. Pierrehumbert, R.T.: Universal short-wave instability of two-dimensional eddies in an inviscid fluid. Phys. Rev. Lett. **57**, 2157 (1986)
32. Platt, N., Sirovich, L., Fitzmaurice, N.: An investigation of chaotic Kolmogorov flows. Phys. Fluids A Fluid Dyn. **3**, 681–696 (1991)
33. Proctor, J.L., Brunton, S.L., Kutz, J.N.: Dynamic mode decomposition with control. SIAM J. Appl. Dyn. Syst. **15**, 142–161 (2016)
34. Provansal, M., Mathis, C., Boyer, L.: Bénard-von Kármán instability: transient and forced regimes. J. Fluid Mech. **182**, 1–22 (1987)
35. Reddy, S.C., Henningson, D.S.: Energy growth in viscous channel flows. J. Fluid Mech. **252**, 209–238 (1993)
36. Rowley, C.W.: Model reduction for fluids, using balanced proper orthogonal decomposition. Int. J. Bifurc. Chaos **15**, 997–1013 (2005)
37. Rowley, C.W., Dawson, S.T.M.: Model reduction for flow analysis and control. Annu. Rev. Fluid Mech. **49**, 387–417 (2017)
38. Schmid, P.J.: Nonmodal stability theory. Annu. Rev. Fluid Mech. **39**, 129–162 (2007)
39. Schmid, P.J.: Dynamic mode decomposition of numerical and experimental data. J. Fluid Mech. **656**, 5–28 (2010)
40. Schmid, P.J., Brandt, L.: Analysis of fluid systems: stability, receptivity, sensitivity. Appl. Mech. Rev. **66**, 024803 (2014)
41. Schmid, P.J., Henningson, D.S.: Stability and Transition in Shear flows. Springer, Berlin (2012)
42. Shimada, I., Nagashima, T.: A numerical approach to ergodic problem of dissipative dynamical systems. Prog. Theor. Phys. **61**, 1605–1616 (1979)

43. Sirovich, L.: Turbulence and the dynamics of coherent structures. Part I: coherent structures. Q. Appl. Math. **45**, 561–571 (1987)
44. Skogestad, S., Postlethwaite, I.: Multivariable Feedback Control: Analysis and Design. Wiley, New York (2007)
45. Sontag, E.D.: Mathematical Control Theory: Deterministic Finite Dimensional Systems. Springer, Berlin (2013)
46. Trefethen, L.N., Trefethen, A.E., Reddy, S.C., Driscoll, T.A.: Hydrodynamic stability without eigenvalues. Science **261**, 578–584 (1993)
47. Von Kármán, T.: Über den Mechanismus des Widerstandes, den ein bewegter Körper in einer Flüssigkeit erfährt. Nachrichten von der Gesellschaft der Wissenschaften zu Göttingen, Mathematisch-Physikalische Klasse **1911**, 509–517 (1911)